

Feature Likelihood Score: Evaluating Generalization of Generative Models Using Samples

Marco Jiralerspong^{1 2} Avishek (Joey) Bose^{2 3} Gauthier Gidel^{1 2 4}

Abstract

Deep generative models have demonstrated the ability to generate complex, high-dimensional, and photo-realistic data. However, a unified framework for evaluating different generative modeling families remains a challenge. Indeed, likelihood-based metrics do not apply in many cases while pure sample-based metrics such as FID fail to capture known failure modes such as overfitting on training data. In this work, we introduce the Feature Likelihood Score (FLS), a parametric sample-based score that uses density estimation to quantitatively measure the quality/diversity of generated samples while taking into account overfitting. We empirically demonstrate the ability of FLS to identify specific overfitting problem cases, even when previously proposed metrics fail. We further perform an extensive experimental evaluation on various image datasets and model classes. Our results indicate that FLS matches intuitions of previous metrics, such as FID, while providing a more holistic evaluation of generative models that highlights models whose generalization abilities are under or overappreciated. Code for computing FLS is provided at <https://github.com/marcojira/fls>.

1. Introduction

Data generation and simulation are some of the fastest-growing use cases of deep generative models, with success stories spanning the artificial intelligence spectrum (Karras et al., 2020b; Brown et al., 2020; Wu et al., 2021). Despite the growth of applications—and unlike supervised or reinforcement learning—there is lack of clear consensus on an evaluation protocol that is equally applicable to any generative modeling family. With the wide-spread adoption of deep generative models and the growing concerns

regarding their data privacy (Carlini et al., 2023; Hitaj et al., 2017), especially in high-stakes and industrial production environments, it is critical to not only reliably evaluate the efficacy of generative models beyond sample quality and diversity but also to diagnose potential failure modes such as memorization.

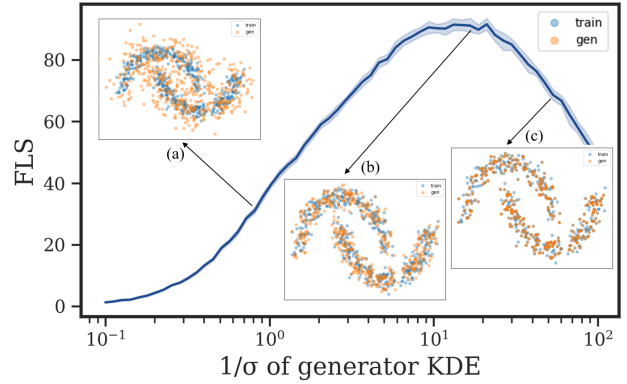


Figure 1. FLS for a generative model that overfits (higher is better). (a) Generated samples are low quality and do not match the underlying Two Moons data \Rightarrow low FLS. (b) Generated samples are high quality, diverse, and are not overfit to the training set \Rightarrow high FLS. (c) Generated samples are still high quality and diverse but too closely resemble the training set \Rightarrow lower FLS.

Current approaches to evaluating generative models are either limited in their applicability to certain model classes (e.g. likelihood) (van den Burg & Williams, 2021) or are one-dimensional scores that miss important facets for evaluation (Xu et al., 2018; Esteban et al., 2017; Meehan et al., 2020). In particular, empirically observed phenomena such as memorization, overfitting, mode collapse, and mode dropping are often overlooked in favor of purely sample quality based metrics such as FID and Inception score. While there exists a body of work (Webster et al., 2019; Alaa et al., 2022; Meehan et al., 2020) dedicated to identifying memorization and overfitting in generative models these themselves have various problems such as being too dependent on nearest neighbor computations or are unable to assess sample quality directly. Thus, at present, there lacks an evaluation measure capable of assessing both sample quality and the generalization capabilities of a generative model.

Current Work. We propose a new sample-based score, the

¹Université de Montréal ²Mila ³McGill University ⁴Canada CIFAR AI Chair. Correspondence to: Marco Jiralerspong <marco.jiralerspong@mila.quebec>.

Feature Likelihood Score (FLS) that captures sample quality, is as scalable as popular sample-based metrics such as FID and Inception score and, crucially, is able to **diagnose overfitting**. Intuitively, FLS is derived from the commonly used likelihood evaluation protocol but is also able to assess the generalization performance of the generative model in a similar manner to most supervised learning setups. Evaluation using FLS has many consequential benefits:

1. **Interpretability:** As scores improve sample quality also improves matching intuition and interpretability.
2. **Diagnosing Overfitting:** As overfitting begins (i.e., memorization of the training set) FLS reports an inferior score *despite* any drop in sample quality and diversity.
3. **Holistic Evaluation:** FLS provides a nuanced evaluation of generative models revealing that some models are overvalued by the FID metric in their (generalization) performance, while many models that have slightly higher FID are better ranked by FLS.
4. **Universal Applicability:** FLS is applicable to all generative models including popular methods like VAEs, Normalizing Flows, GANs, and Diffusion models with minimal overhead as it is computed using only samples.

At an intuitive level, FLS achieves this goal by revisiting the vanilla likelihood metric but in the feature space of a pre-trained Inception-v3 network (Szegedy et al., 2016) or a pre-trained CLIP network (Radford et al., 2021). As most models lack explicit densities, we model the density of the generative model in the feature space by using a mixture of isotropic Gaussians (MoG) whose means are the features of the generated samples. Unlike, conventional likelihood evaluation, FLS is purposely built to diagnose overfitting as it relies on estimating the (perceptual) likelihood of some held-out test data.

Specifically, the key step of our method is that the variance of each isotropic Gaussian is learned by maximizing the likelihood of the set of training examples that were used to train the generative model. Intuitively, the learned Gaussians collapse to Diracs whenever a generated sample is too close to a training example, as illustrated in Fig. 2. We then take advantage of this overfitting by evaluating the log-likelihood of the test set. A model that produces overfit samples will yield an overfit MoG that will have a poor log-likelihood on the test set and hence be punished for its overfitting.

We demonstrate the utility of FLS by conducting extensive experiments across a large variety of generative models for the datasets CIFAR10 (Krizhevsky et al., 2014), Imagenet (Deng et al., 2009), and LSUN (Yu et al., 2015). In particular, we demonstrate that FLS is able to accurately detect overfitting behavior in synthetic settings where other metrics fail 4 while for natural image datasets we show that FLS is well correlated with popular sample-based metrics like FID, demonstrating it is a good judge of sample

quality. In addition, FLS is able to comment on the generalization ability of these trained models both quantitatively and qualitatively, providing an estimate of the degree of overfitting and which samples are the worst offenders. Finally, FLS sheds light on which existing pre-trained models are underrated or overrated by FID—enabling a quantitative appreciation for certain model classes such as DDPM (Ho et al., 2020) while adding additional scrutiny to models like StyleGAN-XL (Sauer et al., 2022).

2. Related Work

The prevalence of deep generative models and their impressive capacity to generate highly realistic data samples has led to the creation of many evaluation metrics.

Likelihood evaluation. The most common metric, and perhaps most natural, is the negative log-likelihood (NLL) of the test set, whenever it is easily computable. While appealing theoretically, in most cases, the generative model doesn’t provide a density (e.g. GANs) or it is only possible to compute a lower bound of the test NLL (e.g. VAEs, continuous diffusion models, etc.) (Burda et al., 2015; Song et al., 2021; Huang et al., 2021). Even when possible, log-likelihood-based evaluation suffers from a variety of pitfalls in high dimensions and may often not correlate with higher sample quality (Nalisnick et al., 2018; Le Lan & Dinh, 2021). Indeed many practitioners have empirically witnessed phenomena such as mode-dropping, mode-collapse, and overfitting (Yazici et al., 2020) all of which are not easily captured simply through the NLL.

Sample-based evaluation. Generative models can also be evaluated purely based on the quality and diversity of their generated samples with popular sample-based metrics such as the Inception score, FID or precision/recall (Salimans et al., 2016; Heusel et al., 2017; Sajjadi et al., 2018). However, a key limitation of these metrics is that they don’t differentiate between good samples and overfit samples.

Overfitting evaluation. Several approaches seek to provide metrics that are capable of detecting overfitting in generative models. These scores can again be categorized based on whether one can extract an exact likelihood (van den Burg & Williams, 2021) or a lower bound to it via annealed importance sampling (Wu et al., 2016). For GANs, popular approaches include training an additional discriminator in a Wasserstein GAN that does not provide gradients to the generator (Adlam et al., 2019) and adding a memorization score to the FID metric (Bai et al., 2021). Alternate approaches to detect overfitting seek to find real data samples that are closest to generated samples via membership attacks (Liu et al., 2018; Webster et al., 2019). Recently, non-parametric tests have been employed to detect memorization or exact data copying in generative models (Xu et al., 2018; Esteban et al.,

2017; Meehan et al., 2020). Parametric approaches to detect data copying have also been explored such as using neural network divergences (Gulrajani et al., 2020) or using latent recovery (Webster et al., 2019). Finally, Alaa et al. (2022) propose a multi-faceted metric with a binary sample-wise test to determine if a sample is authentic or not (i.e. overfit).

3. Evaluation of Generative Models

Given a training dataset $\mathcal{D}_{\text{train}} = \{\mathbf{x}_i\}_{i=1}^n$ drawn from a distribution p_{data} , one of the key objectives of generative modeling is to train a parametric model g that is able to generate novel synthetic yet high-quality samples—i.e., the distribution p_g induced by the generator is close to p_{data} .¹

While some lines of work can evaluate generative models via their density, such an evaluation technique is only possible when one has access to the exact density in a computationally efficient manner of the considered generative model (Song et al., 2021). Moreover, it has been argued that the likelihood of high-dimensional inputs as an evaluation metric for generative models has some major flaws (Theis et al., 2015; Nowozin et al., 2016; Le Lan & Dinh, 2021).

As all deep generative models of interest are capable of producing samples, an effective way to evaluate these models is via their samples. Such a strategy has the benefit of bypassing the need to compute the exact density of a sample point by the model—thus allowing for a unified setting to evaluate all models. More precisely, given $\mathcal{D}_{\text{gen}} = \{\mathbf{x}^{\text{gen}}_i\}_{i=1}^m$ generated samples, where each $\mathbf{x}^{\text{gen}} \sim p_g$ and $\mathcal{D}_{\text{test}} = \{\mathbf{x}^{\text{test}}_i\}_{i=1}^n$ drawn from p_{data} , the goal is to evaluate how “good” the generated samples are with respect to the real data distribution.

3.1. Sample-based metrics

Historically, sample-based metrics for evaluating deep generative models have been based on two ideas: 1) using an Inception network (Szegedy et al., 2016) backbone φ as a feature extractor to 2) compute a notion of distance (or similarity) between the generated and the real distribution. The Inception Score (IS) and the Fréchet Inception Distance are the two most popular examples and can be computed as follows:

$$\text{IS: } \exp\left(\frac{1}{m} \sum_{i=1}^m KL(p_{\varphi}(y|\mathbf{x}_i^{\text{gen}}) || p_d(y))\right) \quad (1)$$

$$\text{FID: } \|\mu_g - \mu_p\|^2 + \text{Tr}(\Sigma_g + \Sigma_p - 2(\Sigma_g \Sigma_p)^{1/2}) \quad (2)$$

where $p_{\varphi}(y|x)$ is the probability of each class given by the Inception network φ , $p(y)$ is the ratio of each class in the real data, $\mu_g := \frac{1}{m} \sum_{i=1}^m \varphi(\mathbf{x}_i^{\text{gen}})$, $\mu_p := \frac{1}{n} \sum_{i=1}^n \varphi(\mathbf{x}_i^{\text{test}})$ are the empirical means of each distribution, and $\Sigma_g := \frac{1}{m} \sum_{i=1}^m (\mathbf{x}_i^{\text{gen}} - \mu_g)(\mathbf{x}_i^{\text{gen}} - \mu_g)^{\top}$, $\Sigma_p := \frac{1}{n} \sum_{i=1}^n (\mathbf{x}_i^{\text{test}} -$

$\mu_p)(\mathbf{x}_i^{\text{test}} - \mu_p)^{\top}$ are the empirical covariances.

The popularity of IS and FID as evaluation metrics for generative models is motivated by their correlation with perceptual quality and diversity. More recently, other metrics such as KID (Binkowski et al., 2018) (an unbiased version of FID) and precision/recall (which disentangles sample quality and distribution coverage) (Sajjadi et al., 2018) have followed in their steps and added additional nuance to generative model evaluation.

However, all the above metrics share the same failure mode: overfitting is not detected. In fact, a trivial generative model that merely memorizes the training set $\mathcal{D}_{\text{train}}$ would get a SOTA score (within statistical uncertainty). This happens regardless of whether it was compared to the training set or the test set. Indeed, the distance between the training set and the test set is negligible compared to the distance between generated samples and the data distribution.

3.2. Feature Likelihood Score

We now introduce our Feature Likelihood Score (FLS) which is predicated on the belief that a proper evaluation measure for generative models should go beyond sample quality and also inform practitioners of the generalization capabilities of their trained models. While previous sample-based methods have foregone density estimation in favor of computing distances between sample statistics, we seek to bring back a likelihood-based approach to evaluating generative models. To do so, we first propose our method for overfitting a mixture of Gaussians (MoGs). Through it, we can estimate the *perceptual* density of high-dimensional samples in a way that accounts for *overfitting*—i.e., samples that are closer to the training data than the test data. Specifically, our method aims at attributing 1) a good density to high-quality, non-overfit images and 2) a very large density to images that have been memorized.

OVERFITTING MIXTURES OF GAUSSIANS

Our method consists of a simple sample-based density estimator amenable to a variety of data domains inspired by a traditional mixture of Gaussians (MoG) density estimator with a few key distinctions. It consists of the following steps:

1. Map the samples to a chosen feature space.
2. Initialize a mixture of Gaussians (MoG) using each mapped sample as a Gaussian.
3. Select individual σ_j^2 for each Gaussian using a set of training samples (also in the feature space).
4. Evaluate log-likelihood of MoG on the test set.

Step 1: Map to feature space. The first change we make is to map the inputs to some perceptually meaningful

¹By close we often refer to either a divergence between the two distributions (e.g. KL, JSD) or a distance metric like Wasserstein.

feature space. A natural choice for this is the representation space of Inception-v3 network but given recent criticisms (Kynkäänniemi et al., 2022), we also experiment with CLIP features. While the resulting data is still high-dimensional (e.g. $d = 2048$ or $d = 512$) we ensure that a larger proportion of dimensions are useful and that the resulting ℓ_2 distances between images are more meaningful.

Step 2: Model the density using an MoG. As in Kernel Density Estimation (KDE), to estimate a density from some set of points $\mathcal{D}_{\text{gen}} = \{\mathbf{x}_j^{\text{gen}}\}_{j=1}^m$ we center an isotropic Gaussian around each point—i.e., the mean of the Gaussian is the coordinates of the point. This means that j -th data point has a Gaussian $\mathcal{N}(\varphi(\mathbf{x}_j^{\text{gen}}), \sigma_j^2 I_d)$. Then, to compute the likelihood of a new point \mathbf{x} , we simply calculate the mean likelihood assigned to that point by all Gaussians in the mixture:

$$p_\sigma(\mathbf{x}) = \frac{1}{m} \sum_{j=1}^m \mathcal{N}(\varphi(\mathbf{x}) | \varphi(\mathbf{x}_j^{\text{gen}}), \sigma_j^2 I_d) \quad (3)$$

with the convention that $\mathcal{N}(\varphi(\mathbf{x}) | \varphi(\mathbf{x}^{\text{gen}}), 0_d)$ is a dirac at $\varphi(\mathbf{x}^{\text{gen}})$. Henceforth, we denote this MoG estimator which has fixed centers initialized to a dataset (e.g. train set, generated set) as $\mathcal{N}(\varphi(\mathcal{D}); \Sigma)$, where Σ is a diagonal matrix of bandwidths parameters—i.e. $\sigma^2 I$, where σ^2 is a vector.

Step 3: Use the train set to select σ_j^2 . An important question in kernel density estimation is selecting an appropriate bandwidth σ_j^2 . Overwhelmingly, a single bandwidth is selected which can either be derived statistically or by minimizing some loss through cross validation (Murphy, 2012). We depart from this single bandwidth philosophy in favor of separate σ_j^2 values for each Gaussian. To select σ_j^2 , instead of performing standard cross-validation on samples from p_g , we fit the bandwidths using a subset of training examples $\{\varphi(\mathbf{x}_i^{\text{train}})\}_{i=1}^n$ by minimizing their negative log-likelihood. Specifically, we solve the following optimization problem:

$$\hat{\sigma} \in \arg \max_{\sigma^2} \sum_{i=1}^n \log \sum_{j=1}^m \sigma_j^{-d} \exp \left(\frac{-\|\varphi(\mathbf{x}_j^{\text{gen}}) - \varphi(\mathbf{x}_i^{\text{train}})\|^2}{2\sigma_j^2} \right) \quad (4)$$

We motivate using a subset of $\{\mathbf{x}_i^{\text{train}}\}_{i=1}^n$ for bandwidth selection as for each element of the training set copied by the generative model, the associated σ_j^2 is vanishing. The following proposition (proof in §E) formalizes this intuition.

Proposition 1. *For each $\mathbf{x}_k^{\text{gen}} \in \{\mathbf{x}_i^{\text{train}}\}_{i=1}^n$ we have that $\hat{\sigma}_k^2 = 0$ where $\hat{\sigma}^2$ is a solution of Eq. 4.*

Proposition 1 implies that each element of the training set that has been memorized induces a Dirac in the MoG density Eq. 3. Thus, the learned density is able to identify copying of training samples. More generally, if

one of the generated samples is unreasonably close to a training sample, its associated σ^2 will be very small as this maximizes the likelihood of the training sample. We illustrate this phenomenon with the Two-Moons dataset (Pedregosa et al., 2011) in Figure 2. Note that since this dataset is low-dimensional, we do not need to use a feature extractor (Step 1). In Figure 2 we can see that the more approximate copies of the training set appear in the generated set, the more the estimated density (using Eq. 4) contains high values around “copies” of the training set. As such, overfit generated samples yield an overfit MoG that does not model the distribution of real data p_{data} and will yield poor (i.e., low) log-likelihood on the test set $\mathcal{D}_{\text{test}}$.

Step 4: Evaluate MoG density. To get a quantitative evaluation of the density obtained in Step 3, we evaluate the likelihood of the $\mathcal{D}_{\text{test}}$ under $p_{\hat{\sigma}}(\mathbf{x})$. As demonstrated in Figure 2, in settings with $k > 0$, the generated samples are too close to the training set meaning that all test samples will have a low likelihood (as they are far from the center of Gaussians with low variances). Evaluation of the test set provides a succinct way of measuring the generalization performance of our generative model which is a key aspect that is lost in metrics such as IS and FID.

It is important to note that while it is indeed possible to train any other density model, an MoG offers a favorable tradeoff in being simple and scalable to large datasets while being highly interpretable as we optimize for each σ_j^2 . Furthermore, a MoG density estimator is universal (Nguyen et al., 2020).

FLS COMPUTATION

Now that we’ve established our method of density estimation for high-dimensional settings, we detail how to use it to compute our FLS score.

FLS is designed to provide a single score that takes into account **sample quality** (IS, precision, etc.), **sample diversity** (FID, recall) while also punishing generative models that **overfit**. To compute our FLS score we use 3 sets of samples: the training set (20000 samples), the test set (10000 samples), and a set of generated samples (10000 samples).

Unless indicated otherwise, for our experiments we used the number of samples given in parentheses. We experimented with larger amounts of samples but this had a minimal impact on score values. We then map all the samples to the chosen feature space (Inception v3 or CLIP).² Once mapped, we normalize the features to have 0 mean and unit variance before computing our scores.

We start by taking the training set and splitting it ran-

²FLS can theoretically be used in any domain with any method for mapping inputs to a meaningful feature space. An investigation of this is beyond the scope of this paper.

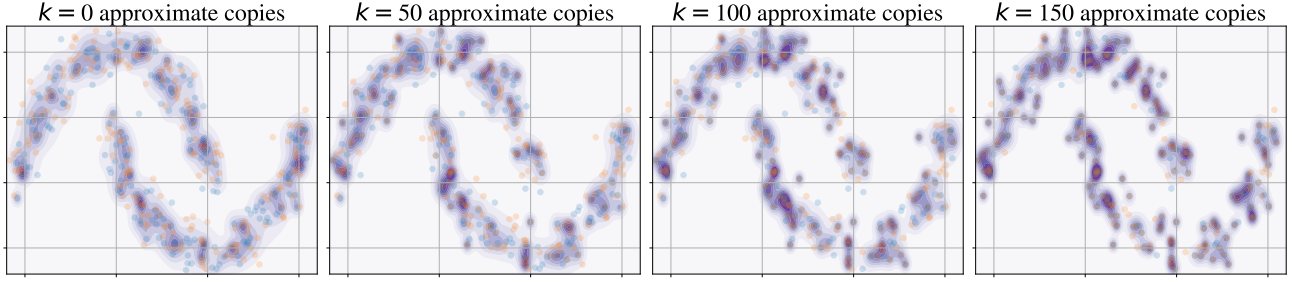


Figure 2. Estimated density (in purple) of the generated distribution using an MoG centered at the generated samples $\mathbf{x}_i^{\text{gen}}$ (in blue) Eq. 3. The selection of σ_i^2 is done via Eq. 4. The training points $\mathbf{x}_i^{\text{train}} \sim p_d$, sampled from the two-moons dataset, are represented in orange. The generated points correspond to k approximates copies of the training set $\mathbf{x}_i^{\text{gen}} = \mathbf{x}_i^{\text{train}} + \mathcal{N}(0, 10^{-4})$, $i = 1, \dots, k$ and $200 - k$ independent samples from the data distribution $\mathbf{x}_i^{\text{gen}} \sim p_d$, $i = k + 1, \dots, 200$. The dark areas correspond to high-density values.

Algorithm 1 Fitting MoGs for FLS

Inputs: $\hat{\mathcal{D}}_{\text{train}}, \mathcal{D}, \varphi, \alpha$

Train. Fit MoG on $\hat{\mathcal{D}}_{\text{train}}$ with $\mu = \varphi(\mathcal{D})$

- 1: $\Sigma = \sigma^2 I$ {// Initialize all bandwidths $\sigma_j^2 = 1$ }
- 2: $\mathbb{H} = d(\varphi(\hat{\mathcal{D}}_{\text{train}}), \varphi(\mathcal{D}))$ {// Pre-compute distance matrix.}
- 3: **while** σ^2 not converged **do**
- 4: $\mathcal{L} = -\log \mathcal{N}(\varphi(\hat{\mathcal{D}}_{\text{train}}) | \varphi(\mathcal{D}); \Sigma)$
- 5: $\sigma^2 \leftarrow \sigma^2 - \alpha \nabla_{\sigma^2} \mathcal{L}$ {// Gradient descent on NLL }
- 6: **end while**
- 7: $\hat{\Sigma} \leftarrow \hat{\sigma}^2 I$ {// $\hat{\sigma}^2$ is the bandwidth at convergence}
- 8: **return** $\mathcal{N}(\varphi(\mathcal{D}); \hat{\Sigma})$ {// Return Trained MoG}

$nll_{\text{baseline}} = \log \mathcal{N}(\varphi(\mathcal{D}_{\text{test}}) | \varphi(\mathcal{D}_{\text{baseline}}); \hat{\Sigma}_{\text{baseline}})$ respectively. **FLS is then defined as:**

$$\text{FLS}(\mathcal{D}_{\text{gen}}) := \exp \left(2 \frac{nll_{\text{baseline}} - nll_{\text{gen}}}{d} \right) \times 100. \quad (5)$$

where d is the dimension of the feature space. This is equivalent to looking at the d^{th} root of the likelihood ratio. A visual depiction of the process is provided in Fig. 3. Intuitively, the score can be considered as a grade with a value of 100 indicating a “perfect” generative model that does as well as a set of samples drawn from the data distribution. Lower values are indicative of problems in some of the three areas evaluated by FLS. Poor sample quality will lead to Gaussian centers that are far from the test set and thus a lower likelihood. A failure to sufficiently cover the data manifold will lead to some test samples having very low likelihoods. Finally, overfitting to the training set will yield the MoG density estimator to overfit and yield a bad likelihood value on the test set.

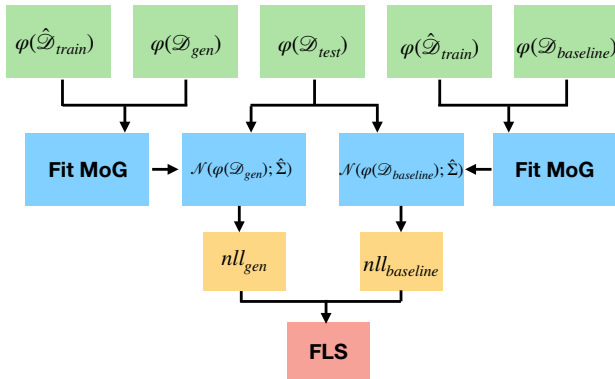


Figure 3. Computation procedure for FLS.

domly into two even subsets, $\mathcal{D}_{\text{train}} = \hat{\mathcal{D}}_{\text{train}} \cup \mathcal{D}_{\text{baseline}}$. The first half $\hat{\mathcal{D}}_{\text{train}}$ will be used to fit the MoG density estimator while the second half $\mathcal{D}_{\text{baseline}}$ will act as our baseline. Assuming that the training set and testing set are drawn i.i.d. from p_{data} , the second subset $\mathcal{D}_{\text{baseline}}$ serves as a reasonable proxy for samples generated by a perfect generative model. We then fit two MoG density estimators to $\hat{\mathcal{D}}_{\text{train}}$. The first, $\mathcal{N}(\varphi(\mathcal{D}_{\text{gen}}); \hat{\Sigma}_{\text{gen}})$, uses the generated samples as centers while the second, $\mathcal{N}(\varphi(\mathcal{D}_{\text{baseline}}); \hat{\Sigma}_{\text{baseline}})$ uses the second half of the train data as centers—i.e. $\varphi(\mathcal{D}_{\text{baseline}})$. The training procedure for the MoG is outlined in Algorithm 1. Finally, we evaluate the log-likelihood of $\mathcal{D}_{\text{test}}$ under both MoGs which we denote as $nll_{\text{gen}} = \log \mathcal{N}(\varphi(\mathcal{D}_{\text{test}}) | \varphi(\mathcal{D}_{\text{gen}}); \hat{\Sigma}_{\text{gen}})$ and

4. Experiments

We investigate the application of FLS on generative models that span a broad category of model families, including popular GAN, Diffusion, and VAE-based generative models. For datasets, we train our models on both toy datasets such as Two Moons (Pedregosa et al., 2011), as well as popular natural image, benchmarks in CIFAR10 (Krizhevsky et al., 2014), Imagenet (Deng et al., 2009), LSUN (Yu et al., 2015), and AFHQ (Choi et al., 2020).

Baselines. Throughout our experiments, we rely on three representative baseline metrics to evaluate generative models: FID, C_T score (Meehan et al., 2020), and AuthPct. These baselines all have the benefit of being sample-based evaluation metrics and allow for a fair comparison with FLS. The C_T is a Mann-Whitney test on the distribution of distances between generated and train samples compared to the distribution of distances between train samples and test samples (negative implies overfit, positive implies

underfit). The $\text{AuthPct} \in [0, 100]$, derived from authenticity described in (Alaa et al., 2022), is simply the percentage of generated samples deemed authentic by their metric (i.e., whose distance to their nearest neighbor in the train set is larger than the distance between that nearest neighbor and its nearest neighbor in the train set).

Our experiments seek to answer the following questions:

- (Q1) **Detecting overfitting in low dimensions.** Does FLS detect overfitting in low-dimensional settings?
- (Q2) **Detecting overfitting in high dimensions.** Does FLS detect overfitting in high-dimensional settings?
- (Q3) **Difference with existing metrics.** How does FLS compare to existing evaluation metrics?

4.1. Detecting overfitting in low dimensions (Q1)

Overfitting on Two Moons. We consider two generative models trained on the Two Moons dataset. The first model is a KDE with the kernel means set to the training set points (visualized in Fig. 2), but the bandwidth σ varies from low to high. For our second model, we train a simple GAN with minor modifications, e.g., large batch sizes, to encourage it to overfit. In Fig. 4, we plot our FLS and all baselines throughout training. As expected, the FLS is near zero for low levels of σ , indicating a high degree of overfitting. However, as σ increases, so does FLS as the samples become less and less overfit before finally starting to drop as the problem shifts from overfitting to underfitting. As such, FLS matches the ability of the C_T score and AuthPct, to discern overfitting when σ is low while also providing an evaluation of sample quality as σ increases. Similarly, for the GAN model, we find that FLS provides a good measure of the improvement in sample quality as the GAN learns the distribution. Eventually, as the GAN begins to overfit, FLS decreases (even though sample quality and diversity remain high).

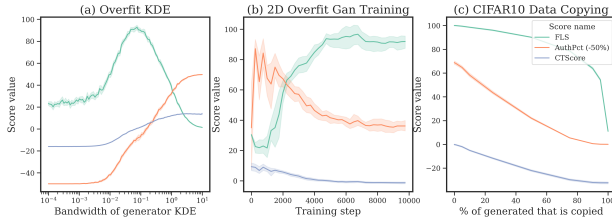


Figure 4. Comparison of metrics on synthetic examples.

4.2. Detecting overfitting in high dimensions (Q2)

Data Copying on CIFAR10. We now study the effect of exact-data copying on CIFAR10, a high-dimensional setting that necessitates mapping inputs to a feature space. We construct a synthetic-generated set with “perfect” quality and diversity but with some memorized training examples. We do so by creating a mixture of the validation set and the training set. We add a small amount of noise to the features of the copied training examples as perfectly exact copies are

unlikely. Intuitively, increasing the proportion of training examples in our synthetic-generated set corresponds to more overfitting/memorization. We report our results in Fig. 4 and observe that FLS decreases as the number of copied/memorized examples increases. The less drastic decrease relative to other metrics is due to the impact of sample quality. Indeed, even with a high percentage of copied samples, the generated samples still contain a large amount of high-quality/diversity samples.

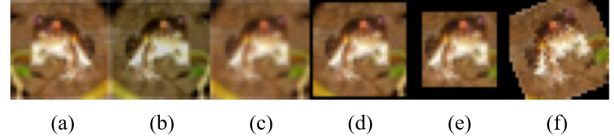


Figure 5. Visualized examples of the transformations.

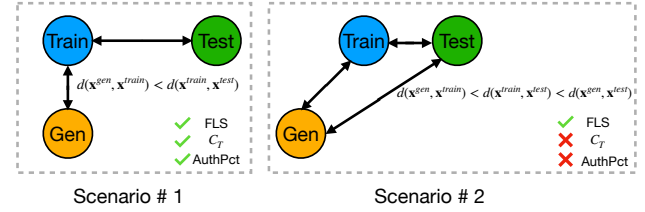


Figure 7. When generated samples are far from both the train and test set (relative to the distance between the train and test sets) but closer to the train set, overfitting is identified by FLS but not by the baselines.

Transformed Data Copying on CIFAR10. We now consider a slightly more realistic scenario than nearly exact data copying by applying image transformation to each copied example. We experiment with popular data augmentation techniques—e.g., cropping, blurring, color jitter, and rotations—as our main image transformation methods (see. Fig. 5). Tab. 1 summarizes our findings. For all transformations, FLS correctly decreases as there are more copied training samples in the pseudo-generated. However, we find the baselines fail to detect overfitting for transformations center crop and random rotation. This failure to capture overfitting can, in part, be explained by both of these scores examining whether generated samples are too close to the training set and not whether they are closer to the training set than they are to the test set (see Fig. 7).

Detecting overfitting. We now investigate the overfitting capabilities of deep generative models on natural image datasets. We start by attempting to disentangle the impact of overfitting on FLS by examining each fitted Gaussian and computing the difference between the train and test log-likelihoods under each Gaussian,

$$\mathcal{O}_i = \log \mathcal{N}(\mathcal{D}_{\text{train}} | x_i; \hat{\sigma}_i^2 I) - \log \mathcal{N}(\mathcal{D}_{\text{test}} | x_i; \hat{\sigma}_i^2 I). \quad (6)$$

If \mathcal{O}_i is positive, we deem the Gaussian overfit. Calculating

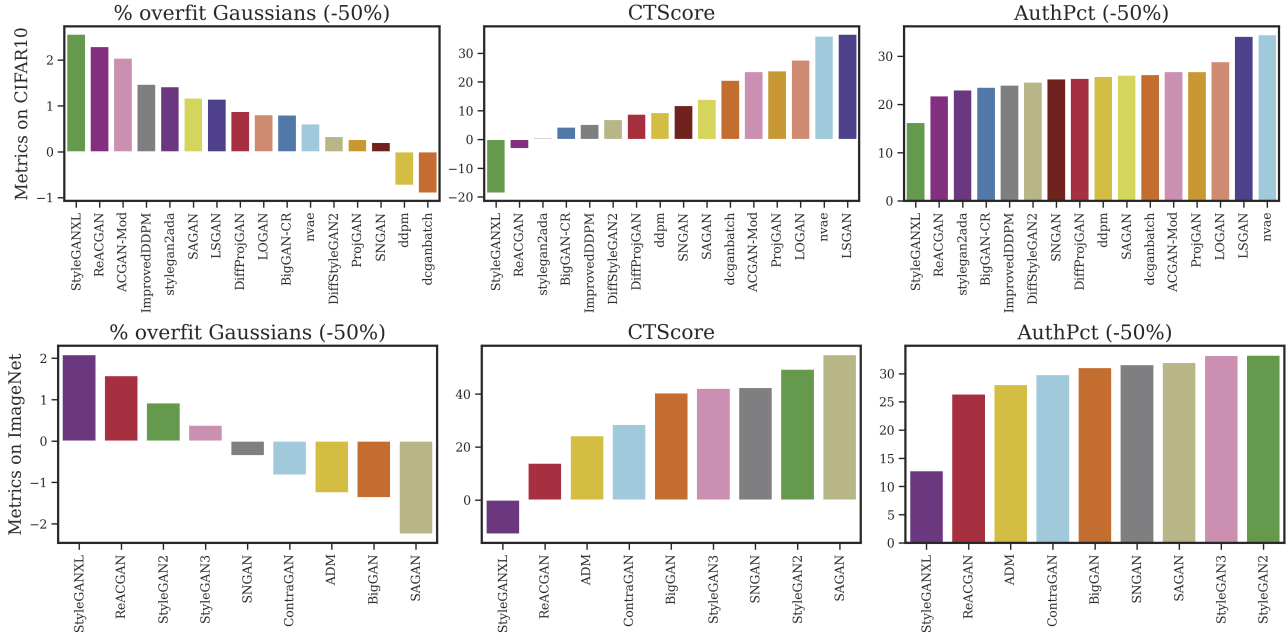


Figure 6. Overfitting score comparison for CIFAR10 and Imagenet generative models. **Left:** Computing \mathcal{O} after standardization by subtracting by 50%. **Mid and Right:** C_T score and AuthPct (also -50%) on various deep generative models.

Table 1. Detection of overfitting by various scores for a model that produces $\mathcal{D}_{\text{transformed}}$, a set of transformed copies of the training set. $\Delta_{\text{score}} = \text{score}(\mathcal{D}_{\text{baseline}}) - \text{score}(\mathcal{D}_{\text{transformed}})$.

TRANSFORMATION	$\Delta_{\text{FLS}} \uparrow$	$\Delta_{\text{CTSCORE}} \uparrow$	$\Delta_{\text{AUTHPCT}} \uparrow$
HORIZONTAL FLIP (A)	66.8 ✓	71.5 ✓	72.8 ✓
GAUSSIAN BLUR (B)	65.3 ✓	66.9 ✓	72.6 ✓
COLOR JITTER (C)	25.4 ✓	48.5 ✓	65.0 ✓
CENTER CROP 30 (D)	19.3 ✓	20.1 ✓	46.7 ✓
CENTER CROP 24 (E)	21.0 ✓	-21.5 ✗	-0.5 ✗
RANDOM ROTATION (F)	17.3 ✓	-16.6 ✗	-6.6 ✗

the percentage of overfit Gaussians gives us a proxy measure of the impact of overfitting on the final FLS value. We expect $\text{FLS} \approx 50\%$ when there is no overfitting and rise linearly with the amount of overfitted samples. Quantitatively, we perform a large-scale evaluation of overfitting in 6, evaluating \mathcal{O}_i , C_T score and AuthPct on a variety of models and datasets. Interestingly, StyleGANXL (Sauer et al., 2022) is deemed to overfit on both datasets, an observation that the C_T score and AuthPct corroborates. In addition, using FLS, we find varying degrees of overfitting behavior for other standard generative models in a similar fashion as C_T score and AuthPct.

We also qualitatively evaluate these findings by comparing the discrepancy between training and test likelihoods under each Gaussian—i.e., \mathcal{O}_i —in the generated samples. By ranking them, we achieve an ordering over the generated samples that have the highest to lowest contribution to overfitting. Using this as a tool, we visualize the overfitting behavior of standard deep generative models on CIFAR10 and Imagenet in Fig. 6. Interestingly, we find different

candidates for “overfit” samples than simply looking at nearest-neighbors (as depicted in 8). It is likely that an overfit sample will resemble a bunch of different training samples, borrowing a bit from each instead of just being close to one of them, a subtlety that is captured by FLS and not nearest-neighbor-based evaluations.

4.3. Difference and Correlation with FID (Q3)

We now investigate the relationship between FLS and FID, performing a large-scale comparison of the same set of models and datasets. For CIFAR 10 and Imagenet, we plot FLS vs. FID in Fig 9 respectively and conduct a simple linear regression analysis. A corresponding plot for LSUN is presented in Appendix §A.1. Overall, we find evidence of a strong correlation between FLS and FID for all datasets, which highlights that FLS captures sample quality/diversity as well. However, despite this correlation, by inspecting the residuals of a standard linear regression between FID and FLS, we notice a few clear outliers. In particular, we find that certain models obtain too high of an FID score given their FLS (i.e., “overrated” by FID).

For example, we find that NVAE (Vahdat & Kautz, 2020) is overrated by FID. We reconcile this fact by noting that NVAE samples tend to be more diverse but of lower quality. The discrepancy in scores indicates that, from a likelihood perspective, FLS values sample quality more than FID. We also uncover models that FID underrates. For instance, on CIFAR 10, we find that DCGAN (Radford et al., 2015) is underrated, which we hypothesize is due to the simplicity

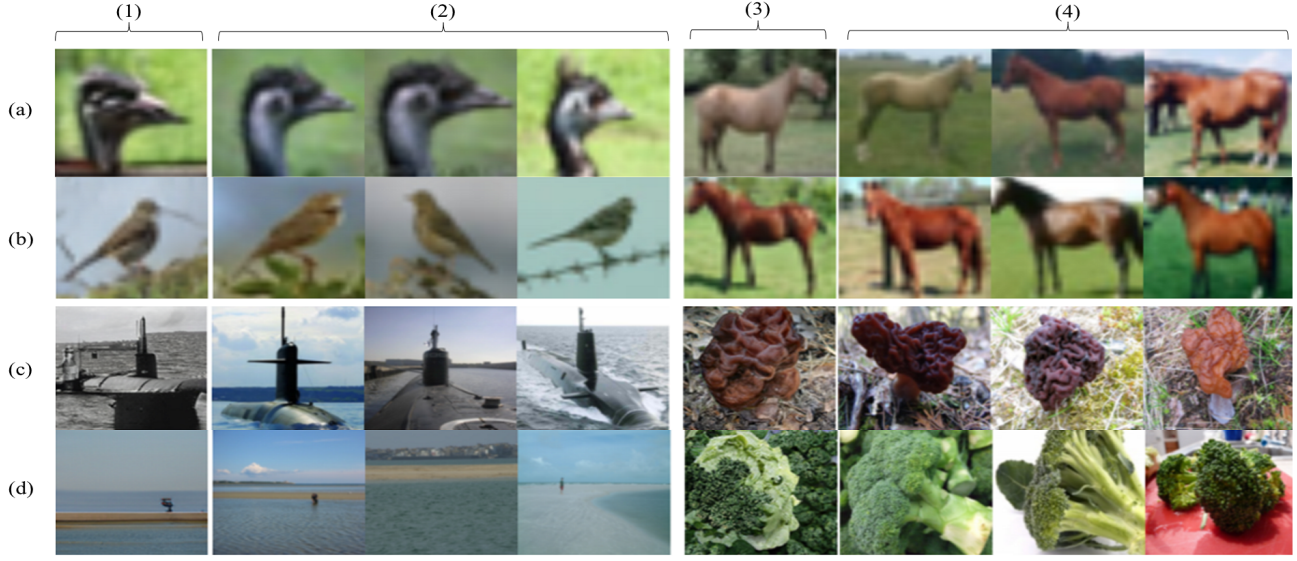


Figure 8. Overfit samples detected using FLS vs Nearest Neighbors, illustrating the more subtle overfitting captured by FLS. (1) is the sample corresponding to the most overfit gaussian while (2) consists of the train samples with the highest likelihood under (1). We compare with (3), the generated sample closest to the training set in ℓ_2 distance, while (4) is the 3 closest training sample. (a) is from BigGAN-CR on CIFAR10, (b) is from DiffStyleGAN2, (c) is from StyleGANXL on Imagenet, and (d) is from ContraGAN.

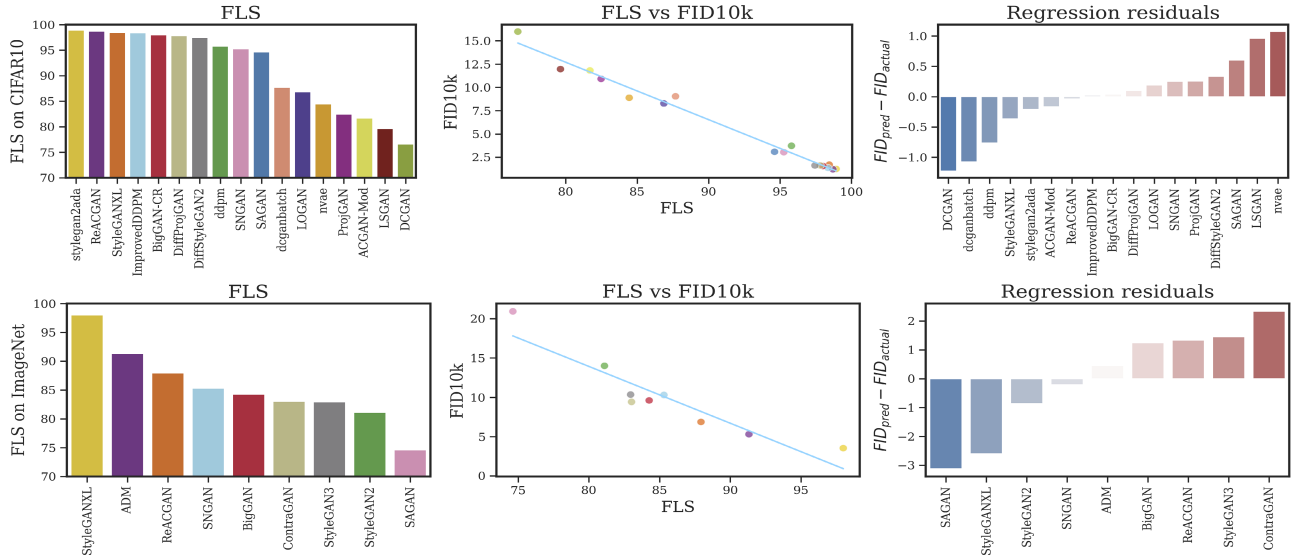


Figure 9. FLS vs FID score comparisons for CIFAR10 and Imagenet.

of the model and the fact that it predates the FID metric and is thus not the result of DCGAN trying to optimize for FID.

5. Conclusion

In this paper, we introduce **FLS**, a new holistic evaluation metric for deep generative models that encompasses many of the key desiderata for a sound evaluation. Specifically, FLS is easy to compute, broadly applicable to all generative models, and evaluates generation quality, diversity, as well as generalization. Moreover, we show that, unlike previous

approaches, FLS provides more insights into trained generative models while being universally applicable to all model families. We empirically demonstrate both on synthetic and real-world datasets that FLS can diagnose important failure modes such as memorization/overfitting—informing practitioners on the potential limitations of generative models that generate photo-realistic images. While we focused on the domain of natural images, a fertile direction for future work is to extend FLS to other data modalities such as text, audio, or time series and also evaluating conditional generative models.

Acknowledgements

The authors would like to thank Ian Gemp, Chongli Qin, and Yoram Bachrach for fruitful discussions. AJB was generously supported by an IVADO Ph.D. fellowship.

References

- Adlam, B., Weill, C., and Kapoor, A. Investigating under and overfitting in wasserstein generative adversarial networks. *arXiv preprint arXiv:1910.14137*, 2019. 2
- Alaa, A., Van Breugel, B., Saveliev, E. S., and van der Schaar, M. How faithful is your synthetic data? sample-level metrics for evaluating and auditing generative models. In *International Conference on Machine Learning*. PMLR, 2022. 1, 3, 6
- Bai, C.-Y., Lin, H.-T., Raffel, C., and Kan, W. C.-w. On training sample memorization: Lessons from benchmarking generative modeling with a large-scale competition. In *Proceedings of the 27th ACM SIGKDD Conference on Knowledge Discovery & Data Mining*, 2021. 2
- Bińkowski, M., Sutherland, D. J., Arbel, M., and Gretton, A. Demystifying mmd GANs. *arXiv preprint arXiv:1801.01401*, 2018. 3
- Brock, A., Donahue, J., and Simonyan, K. Large scale GAN training for high fidelity natural image synthesis. *arXiv preprint arXiv:1809.11096*, 2018. 12, 19
- Brown, T. B., Mann, B., Ryder, N., Subbiah, M., Kaplan, J., Dhariwal, P., Neelakantan, A., Shyam, P., Sastry, G., Askell, A., et al. Language models are few-shot learners. *arXiv preprint arXiv:2005.14165*, 2020. 1
- Burda, Y., Grosse, R., and Salakhutdinov, R. Importance weighted autoencoders. *arXiv preprint arXiv:1509.00519*, 2015. 2
- Carlini, N., Hayes, J., Nasr, M., Jagielski, M., Sehwag, V., Tramèr, F., Balle, B., Ippolito, D., and Wallace, E. Extracting Training Data from Diffusion Models. *arXiv preprint arXiv:2301.13188*, 2023. 1
- Choi, Y., Uh, Y., Yoo, J., and Ha, J.-W. StarGAN v2: Diverse image synthesis for multiple domains. In *Proceedings of the IEEE/CVF conference on computer vision and pattern recognition*, 2020. 5
- Deng, J., Dong, W., Socher, R., Li, L.-J., Li, K., and Fei-Fei, L. Imagenet: A large-scale hierarchical image database. In *2009 IEEE conference on computer vision and pattern recognition*. Ieee, 2009. 2, 5
- Dhariwal, P. and Nichol, A. Diffusion models beat GANs on image synthesis. *Advances in Neural Information Processing Systems*, 34, 2021. 19
- Esteban, C., Hyland, S. L., and Rätsch, G. Real-valued (medical) time series generation with recurrent conditional GANs. *arXiv preprint arXiv:1706.02633*, 2017. 1, 2
- Gulrajani, I., Ahmed, F., Arjovsky, M., Dumoulin, V., and Courville, A. C. Improved training of wasserstein GANs. *Advances in Neural Information Processing Systems*, 30, 2017. 18
- Gulrajani, I., Raffel, C., and Metz, L. Towards GAN benchmarks which require generalization. *arXiv preprint arXiv:2001.03653*, 2020. 3
- Heusel, M., Ramsauer, H., Unterthiner, T., Nessler, B., and Hochreiter, S. GANs trained by a two time-scale update rule converge to a local nash equilibrium. *Advances in Neural Information Processing Systems*, 30, 2017. 2
- Hitaj, B., Ateniese, G., and Perez-Cruz, F. Deep models under the GAN: information leakage from collaborative deep learning. In *Proceedings of the 2017 ACM SIGSAC conference on computer and communications security*, 2017. 1
- Ho, J., Jain, A., and Abbeel, P. Denoising diffusion probabilistic models. *Advances in Neural Information Processing Systems*, 33, 2020. 2, 19
- Huang, C.-W., Lim, J. H., and Courville, A. C. A variational perspective on diffusion-based generative models and score matching. *Advances in Neural Information Processing Systems*, 34, 2021. 2
- Kang, M. and Park, J. ContraGAN: Contrastive learning for conditional image generation. *Advances in Neural Information Processing Systems*, 33, 2020. 19
- Kang, M., Shim, W., Cho, M., and Park, J. Rebooting ACGAN: Auxiliary classifier GANs with stable training. *Advances in Neural Information Processing Systems*, 34, 2021. 18, 19
- Kang, M., Shin, J., and Park, J. StudioGAN: A Taxonomy and Benchmark of GANs for Image Synthesis. 2206.09479 (*arXiv*), 2022. 18, 19
- Karras, T., Aittala, M., Hellsten, J., Laine, S., Lehtinen, J., and Aila, T. Training generative adversarial networks with limited data. *Advances in neural information processing systems*, 33, 2020a. 12, 19
- Karras, T., Laine, S., Aittala, M., Hellsten, J., Lehtinen, J., and Aila, T. Analyzing and improving the image

- quality of styleGAN. In *Proceedings of the IEEE/CVF Conference on Computer Vision and Pattern Recognition*, 2020b. 1, 19
- Karras, T., Aittala, M., Laine, S., Härkönen, E., Hellsten, J., Lehtinen, J., and Aila, T. Alias-free generative adversarial networks. *Advances in Neural Information Processing Systems*, 34, 2021. 19
- Krizhevsky, A., Nair, V., and Hinton, G. The CIFAR-10 dataset. online: <http://www.cs.toronto.edu/kriz/cifar.html>, 2014. 2, 5, 18
- Kynkäänniemi, T., Karras, T., Aittala, M., Aila, T., and Lehtinen, J. The Role of ImageNet Classes in Fréchet Inception Distance. *arXiv preprint arXiv:2203.06026*, 2022. 4
- Le Lan, C. and Dinh, L. Perfect density models cannot guarantee anomaly detection. *Entropy*, 23(12), 2021. 2, 3
- Liu, K. S., Li, B., and Gao, J. Generative model: Membership attack, generalization and diversity. *CoRR*, abs/1805.09898, 3, 2018. 2
- maintainers, T. and contributors. TorchVision: PyTorch’s Computer Vision library. <https://github.com/pytorch/vision>, 2016. 18
- Mao, X., Li, Q., Xie, H., Lau, R. Y., Wang, Z., and Paul Smolley, S. Least squares generative adversarial networks. In *Proceedings of the IEEE international conference on computer vision*, 2017. 18
- Meehan, C., Chaudhuri, K., and Dasgupta, S. A non-parametric test to detect data-copying in generative models. In *International Conference on Artificial Intelligence and Statistics*, 2020. 1, 3, 5
- Miyato, T., Kataoka, T., Koyama, M., and Yoshida, Y. Spectral normalization for generative adversarial networks. *arXiv preprint arXiv:1802.05957*, 2018. 18, 19
- Murphy, K. P. *Machine learning: a probabilistic perspective*. MIT press, 2012. 4
- Nalisnick, E., Matsukawa, A., Teh, Y. W., Gorur, D., and Lakshminarayanan, B. Do deep generative models know what they don’t know? *arXiv preprint arXiv:1810.09136*, 2018. 2
- Nguyen, T. T., Nguyen, H. D., Chamroukhi, F., and McLachlan, G. J. Approximation by finite mixtures of continuous density functions that vanish at infinity. *Cogent Mathematics & Statistics*, 7(1), 2020. 4
- Nichol, A. Q. and Dhariwal, P. Improved denoising diffusion probabilistic models. In *International Conference on Machine Learning*. PMLR, 2021. 12, 19
- Nowozin, S., Cseke, B., and Tomioka, R. f-GAN: Training generative neural samplers using variational divergence minimization. *Advances in Neural Information Processing Systems*, 29, 2016. 3
- Pedregosa, F., Varoquaux, G., Gramfort, A., Michel, V., Thirion, B., Grisel, O., Blondel, M., Prettenhofer, P., Weiss, R., Dubourg, V., et al. Scikit-learn: Machine learning in Python. *the Journal of machine Learning research*, 12, 2011. 4, 5, 18
- Radford, A., Metz, L., and Chintala, S. Unsupervised representation learning with deep convolutional generative adversarial networks. *arXiv preprint arXiv:1511.06434*, 2015. 7, 18
- Radford, A., Kim, J. W., Hallacy, C., Ramesh, A., Goh, G., Agarwal, S., Sastry, G., Askell, A., Mishkin, P., Clark, J., et al. Learning transferable visual models from natural language supervision. In *International conference on machine learning*. PMLR, 2021. 2
- Rombach, R., Blattmann, A., Lorenz, D., Esser, P., and Ommer, B. High-resolution image synthesis with latent diffusion models. In *Proceedings of the IEEE/CVF Conference on Computer Vision and Pattern Recognition*, 2022. 19
- Sajjadi, M. S., Bachem, O., Lucic, M., Bousquet, O., and Gelly, S. Assessing generative models via precision and recall. *Advances in Neural Information Processing Systems*, 31, 2018. 2, 3
- Salimans, T., Goodfellow, I., Zaremba, W., Cheung, V., Radford, A., and Chen, X. Improved techniques for training GANs. *Advances in neural information processing systems*, 29, 2016. 2
- Sauer, A., Chitta, K., Müller, J., and Geiger, A. Projected GANs converge faster. *Advances in Neural Information Processing Systems*, 34, 2021. 18, 19
- Sauer, A., Schwarz, K., and Geiger, A. StyleGAN-xl: Scaling styleGAN to large diverse datasets. In *ACM SIGGRAPH 2022 conference proceedings*, 2022. 2, 7, 18, 19
- Song, J., Meng, C., and Ermon, S. Denoising diffusion implicit models. *arXiv preprint arXiv:2010.02502*, 2020. 19
- Song, Y., Durkan, C., Murray, I., and Ermon, S. Maximum likelihood training of score-based diffusion models. *Advances in Neural Information Processing Systems*, 34, 2021. 2, 3

- Szegedy, C., Vanhoucke, V., Ioffe, S., Shlens, J., and Wojna, Z. Rethinking the inception architecture for computer vision. In *Proceedings of the IEEE conference on computer vision and pattern recognition*, 2016. 2, 3
- Theis, L., Oord, A. v. d., and Bethge, M. A note on the evaluation of generative models. *arXiv preprint arXiv:1511.01844*, 2015. 3
- Vahdat, A. and Kautz, J. NVAE: A deep hierarchical variational autoencoder. *Advances in Neural Information Processing Systems*, 33, 2020. 7, 19
- van den Burg, G. and Williams, C. On memorization in probabilistic deep generative models. *Advances in Neural Information Processing Systems*, 34, 2021. 1, 2
- von Platen, P., Patil, S., Lozhkov, A., Cuenca, P., Lambert, N., Rasul, K., Davaadorj, M., and Wolf, T. Diffusers: State-of-the-art diffusion models. <https://github.com/huggingface/diffusers>, 2022. 19
- Wang, Z., Zheng, H., He, P., Chen, W., and Zhou, M. Diffusion-GAN: Training GANs with diffusion. *arXiv preprint arXiv:2206.02262*, 2022. 19
- Webster, R., Rabin, J., Simon, L., and Jurie, F. Detecting overfitting of deep generative networks via latent recovery. In *Proceedings of the IEEE/CVF Conference on Computer Vision and Pattern Recognition*, 2019. 1, 2, 3
- Wu, Y., Burda, Y., Salakhutdinov, R., and Grosse, R. On the quantitative analysis of decoder-based generative models. *arXiv preprint arXiv:1611.04273*, 2016. 2
- Wu, Y., Donahue, J., Balduzzi, D., Simonyan, K., and Lillicrap, T. LoGAN: Latent optimisation for generative adversarial networks. *arXiv preprint arXiv:1912.00953*, 2019. 18
- Wu, Z., Johnston, K. E., Arnold, F. H., and Yang, K. K. Protein sequence design with deep generative models. *Current Opinion in Chemical Biology*, 65, 2021. 1
- Xu, Q., Huang, G., Yuan, Y., Guo, C., Sun, Y., Wu, F., and Weinberger, K. An empirical study on evaluation metrics of generative adversarial networks. *arXiv preprint arXiv:1806.07755*, 2018. 1, 2
- Yazici, Y., Foo, C.-S., Winkler, S., Yap, K.-H., and Chandrasekhar, V. Empirical analysis of overfitting and mode drop in gan training. In *2020 IEEE International Conference on Image Processing (ICIP)*. IEEE, 2020. 2
- Yu, F., Seff, A., Zhang, Y., Song, S., Funkhouser, T., and Xiao, J. Lsun: Construction of a large-scale image dataset using deep learning with humans in the loop. *arXiv preprint arXiv:1506.03365*, 2015. 2, 5, 12
- Zhang, H., Goodfellow, I., Metaxas, D., and Odena, A. Self-attention generative adversarial networks. In *International conference on machine learning*. PMLR, 2019a. 18, 19
- Zhang, H., Zhang, Z., Odena, A., and Lee, H. Consistency regularization for generative adversarial networks. *arXiv preprint arXiv:1910.12027*, 2019b. 18

A. Additional Results

A.1. LSUN results

We conduct the same experiments found in Q3 for the LSUN dataset (Yu et al., 2015). Specifically, we evaluate the FLS on standard generative models and also perform a linear regression analysis with respect to FID. In Fig. 10 shows our findings where, for example, we observe that the Improved DDPM model (Nichol & Dhariwal, 2021) is underrated by FID in comparison to FLS.

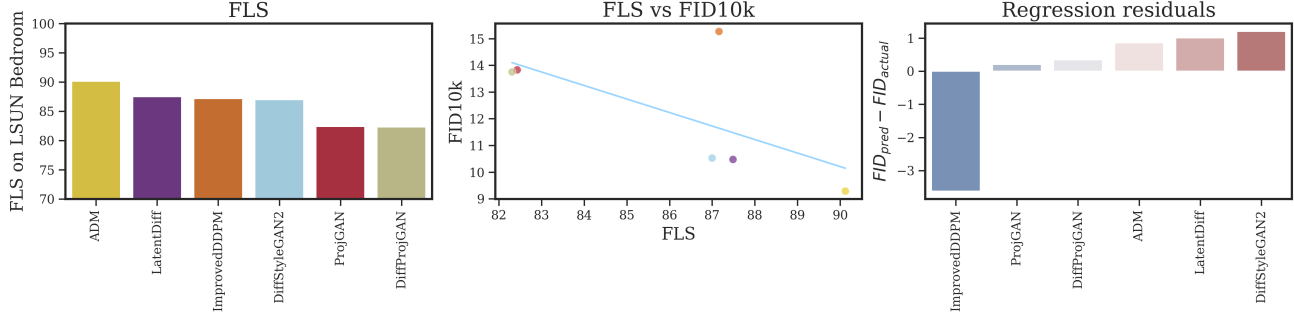


Figure 10. FLS vs. FID for LSUN Bedrooms dataset.

A.2. GAN truncation experiments

We demonstrate the usefulness of a single comprehensive score for hyperparameter selection. For example, as demonstrated by (Brock et al., 2018), truncating the latent space variable you sample from for GANs can increase sample quality at the expense of sample diversity. Through FLS, picking the optimal truncation value for a GAN can be done in a way that trades off naturally between precision/recall. Below are the FID/FLS values for various truncation values of StyleGANXL on Imagenet 128x128 (unconditional). Interestingly, the optimal selected value is lower than FID in both cases, indicating once again that FLS seems to value image quality more highly than FID.

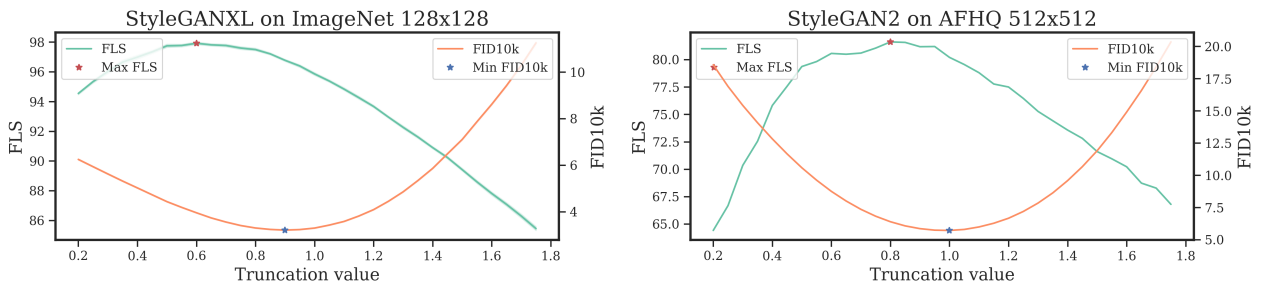


Figure 11. FLS vs. FID for selecting optimal GAN truncation values.

A.3. Overfitting and dataset size

We investigate the impact of dataset size on overfitting. As generative models tend to struggle with small datasets, we start with a pre-trained StyleGAN2-Ada model on FFHQ and fine-tune it on AFHQ (cat), as described in (Karras et al., 2020a). Specifically, we split the training set of AFHQ (cat) into subsets of varying sizes (500, 1000, 2000, 4000) and fine-tune a pre-trained StyleGAN2-Ada model on each subset, using default parameters. We then get the final checkpoints after 72 hours of training and compute FLS, CTScore and AuthPct on the checkpoint of each dataset size (using as training set the subset and not the whole dataset).

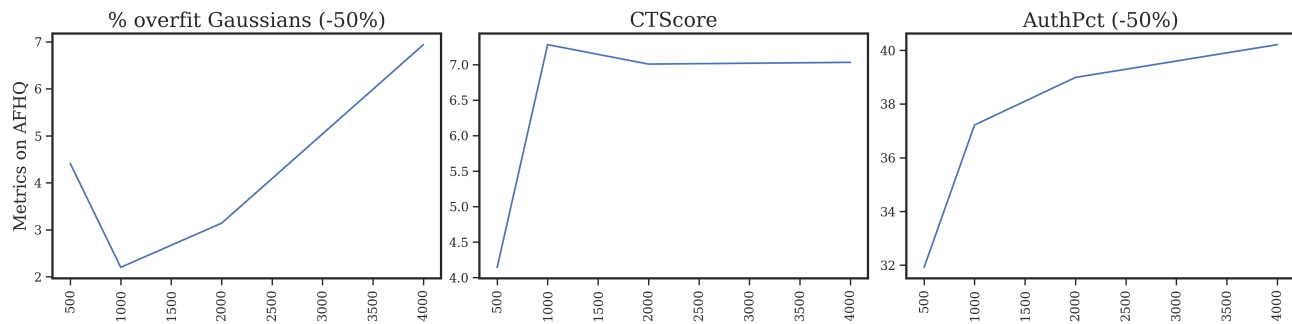


Figure 12. Overfitting metric values for StyleGAN2-Ada trained on various sizes of AFHQ cat. For % overfit Gaussians (-50%), a positive value indicates overfitting while for the other two metrics, a positive value indicates underfitting.

Interestingly, here FLS indicates there is some degree of overfitting whereas the two other metrics signal that the models are underfit. The discrepancy can potentially be the same reason provided for the transforms experiment. Due to the relatively small sizes of the train and test sets, it is possible that the generated samples are far from both which leads CTScore and AuthPct to consider them "underfit". We also investigate qualitatively below, using the overfit Gaussian methodology used previously and find evidence of overfit samples that combine the color of some training samples and the pose of others.



Figure 13. Overfit samples on AFHQ. Each row corresponds to the most overfit sample for some model, the leftmost image being the generated sample. The 8 images on the right are the samples in the train set with the highest likelihood for the Gaussian corresponding to that sample. From top to bottom: 500 training samples, 1000 training samples, 2000 training samples, 4000 training samples.

B. Additional overfit samples

Below are additional overfit samples detected from various models/datasets.

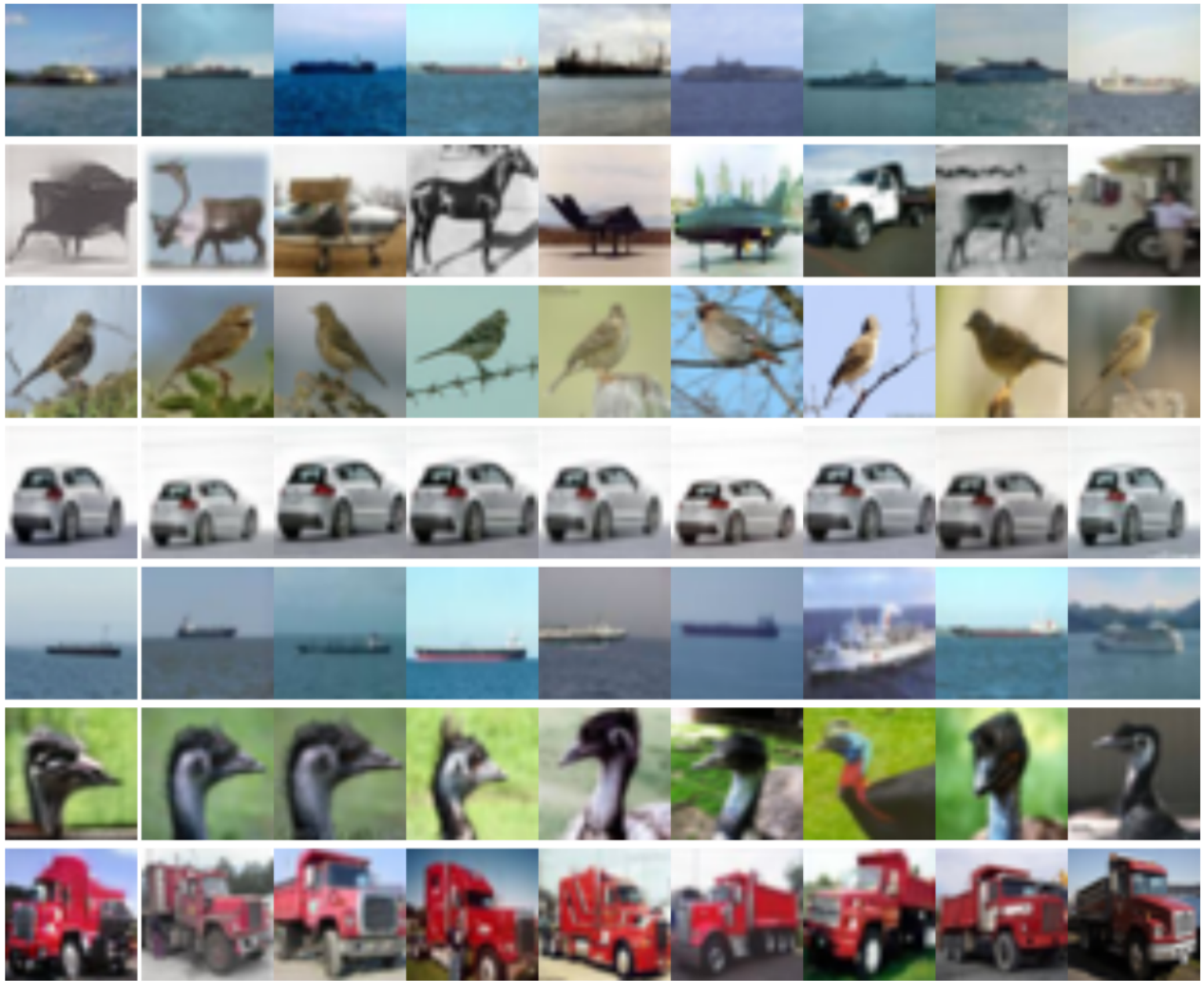


Figure 14. Overfit samples for CIFAR10. Each row corresponds to the most overfit sample for some model, the leftmost image being the generated sample. The 8 images on the right are the samples in the train set with the highest likelihood for the Gaussian corresponding to that sample. From top to bottom: DDPM, NVAE, DiffStyleGAN2, ImprovedDDPM, StyleGANXL, BigGAN-CR, ReACGAN

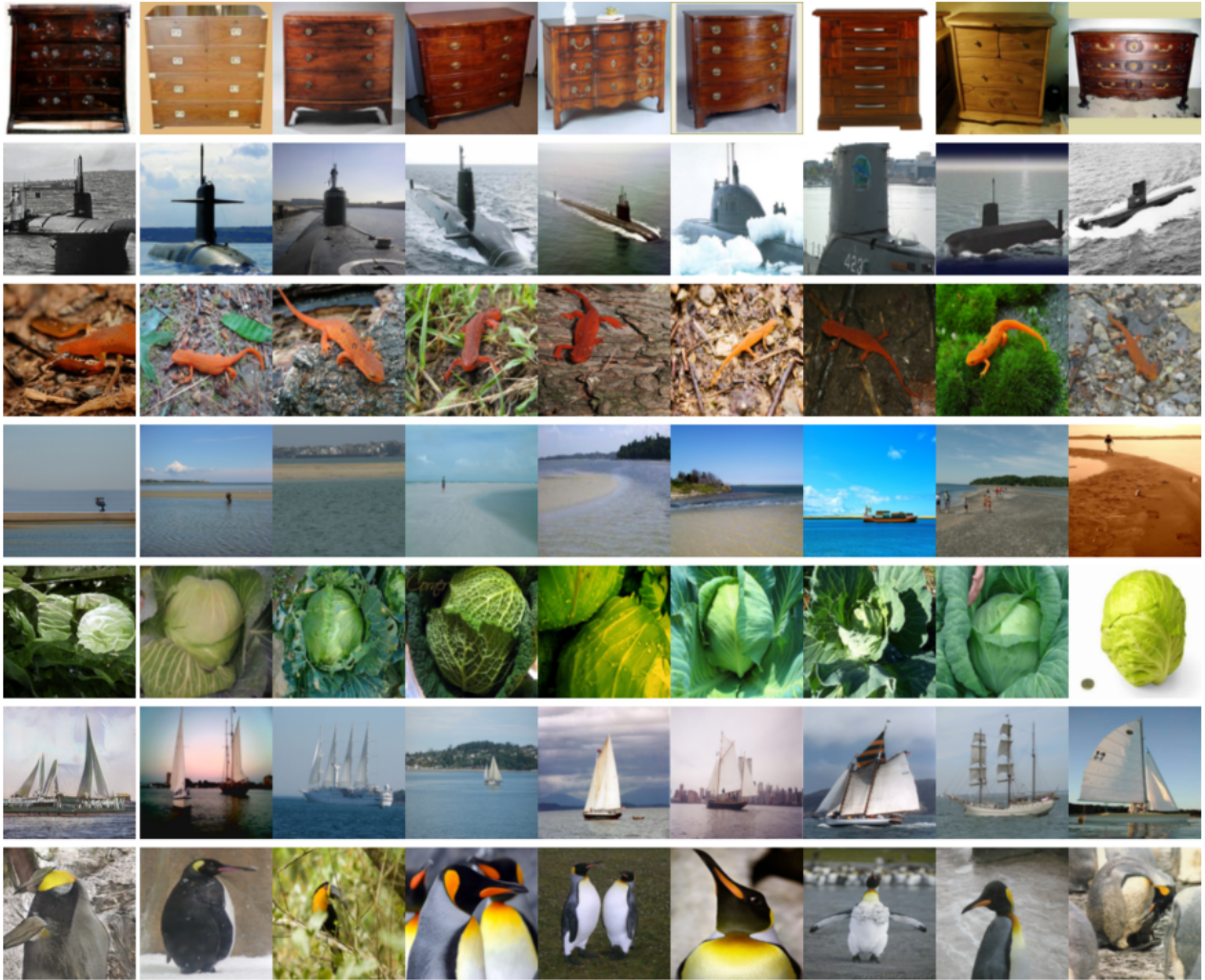


Figure 15. Overfit samples on ImageNet. Each row corresponds to the most overfit sample for some model, the leftmost image being the generated sample. The 8 images on the right are the samples in the train set with the highest likelihood for the Gaussian corresponding to that sample. From top to bottom: ADM, StyleGANXL, ContraGAN, SNGAN, StyleGAN2, StyleGAN3

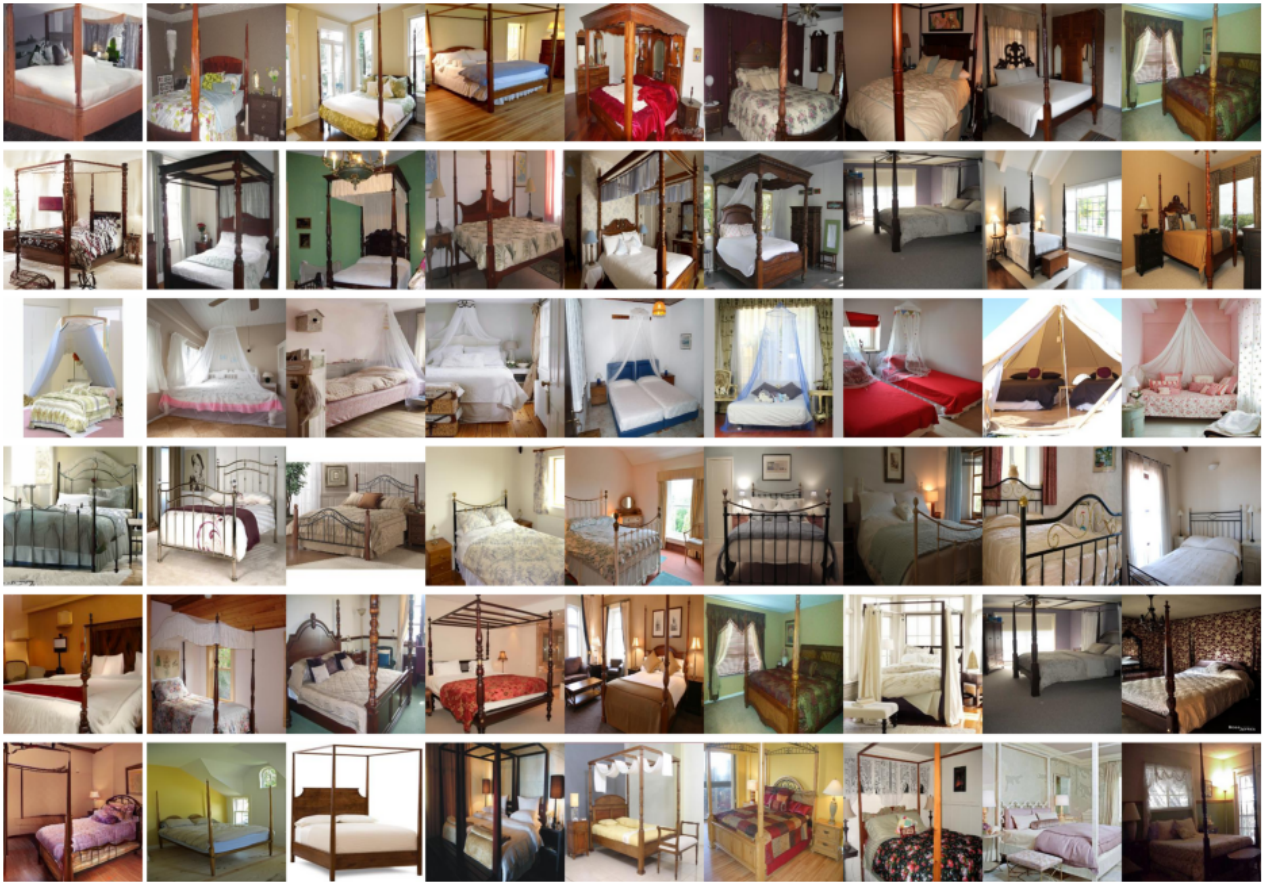


Figure 16. Overfit samples on LSUN Bedroom. Each row corresponds to the most overfit sample for some model, the leftmost image being the generated sample. The 8 images on the right are the samples in the train set with the highest likelihood for the Gaussian corresponding to that sample. From top to bottom: DiffProjGAN, DiffStyleGAN2, ADM, ImprovedDDPM, LatentDiff, ProjGAN

C. Optimization procedure

Selecting σ_j for each generated sample by solving the optimization problem 4 is non-trivial. Even with the simplifying assumption of a diagonal covariance matrix, we still need to learn one parameter per Gaussian (of which there are 10000). As the likelihood of given points comes from the log of the sum of individual Gaussians, the σ_j cannot be optimized independently. Thus, we turn to full batch gradient descent using the Adam optimizer with the following hyperparameters:

- 100 steps
- $lr = 0.5$
- Initial value for log variance: 0
- We use a 2-step lr scheduler, reducing the learning rate by a factor of 10 after 50 steps.

In addition, getting the likelihood assigned by each Gaussian to each point requires computing the distance between each pair $(\mathbf{x}_i^{\text{gen}}, \mathbf{x}_i^{\text{train}})$ which is $O(n^2)$ and time-consuming. As the distances and dimensions are large (at least for our high-dimensional experiments), the exponentiation and summations were often numerically unstable. To address this, we:

- Compute the $O(n^2)$ distance matrix once and store it so as not to recompute it for each step of the optimization procedure.
- Optimize the log variances instead of the variances themselves
- Convert σ_j^{-d} to $\exp(-d \times \log(\sigma_j))$ to be able to take advantage of a numerically stable logsumexp.

From plotting the loss, the variances almost always converged in short order (usually less than 20 steps). While we have no guarantee that these were global minima, when there were exact copies or close to exact copies, 1 would recover very low log variances, as shown in 1.

D. Experimental Setup

D.1. Detecting overfitting in low dimensions

For the overfit KDE experiment, we generate 3000 points from the Two Moons dataset using scikit-learn (Pedregosa et al., 2011) with a noise value of 0.1. The first 2000 points are used as the training set and the last 1000 as test set. We fit a KDE to the train set using bandwidth values varying from 10^{-4} to 10 and sample 1000 points as generated samples before computing our score.

As for the GAN, we use a simple 2 layer fully connected generator and discriminator with ReLU activations. We generate 1000 samples (less than above to better be able to visually see the difference between the train and test sets) with the same 0.1 noise value. The first 500 are used as train set and the last 500 as test set. We train for 10000 steps using full batch gradient descent (learning rate of $1e-2$) on the training set with a fixed value of the latent variable z for the generated samples (to encourage it to overfit). Finally, the generated samples of that fixed z are the generated samples.

D.2. Detecting overfitting in high dimensions

Data copying. We take 3 separate batches of 10000 samples from the CIFAR10 (Krizhevsky et al., 2014) train set and the entire test set. The first is used as "training set" for the purposes of our score computation, the second as validation set and the last as baseline set. The "generated samples" are a mixture of the validation set and increasingly more samples from the "training set" (with a Gaussian noise of 0.1 added in the feature space). Finally, we get score values with respect to the test set.

Simple transforms. We use standard torchvision (maintainers & contributors, 2016) image transforms applied to the "training set" above and repeat the same process:

- **Horizontal flip:** The image is flipped horizontally.
- **Gaussian blur:** Gaussian blur with a (5, 5) kernel and a σ of 0.5.
- **Horizontal Flip:** Color jitter transform with blur in [0.6, 1.4], contrast in [0.6, 1.4], saturation in [0.6, 1.4] and hue in [-0.05, 0.05].
- **Center crop 30:** Center crop the image to (30, 30) and fill the rest with black.
- **Center crop 24:** Center crop the image to (24, 24) and fill the rest with black.
- **Random rotation:** Random rotation between [0, 45] degrees.

D.3. Large scale model comparison

For model comparison, we either use pre-trained networks provided by the respective paper authors OR pre-trained networks provided by StudioGAN (Kang et al., 2022), a very impressive library that reproduces a large array of GAN models.

We generate 10000 samples for each. Due to the computational requirements of generating samples from diffusion models (often 2 orders of magnitude higher than GANs), we resort to lowering the number of steps during sampling with aggressive timestep respacing. It is likely that with more steps, diffusion models would achieve even higher FLS values.

CIFAR10 models.

- **StudioGAN** (Kang et al., 2022): We take the pre-trained models provided here. Specifically, if there are multiple training runs, we take the latest one and use the weights from the best checkpoint. The models that were reproduced by StudioGAN that we used are: DCGAN (Radford et al., 2015), WGAN-GP (Gulrajani et al., 2017), SNGAN (Miyato et al., 2018), SAGAN (Zhang et al., 2019a), ReACGAN (Kang et al., 2021), ProjGAN (Sauer et al., 2021), LSGAN (Mao et al., 2017), LOGAN (Wu et al., 2019), BigGAN-CR (Zhang et al., 2019b) and ACGAN-Mod (Kang et al., 2021).
- **StyleGANXL** (Sauer et al., 2022): We use the pre-trained model provided here and generate 10000 samples (seeds 0 – 10000).

- **StyleGAN2-ada** (Karras et al., 2020a): We use the pre-trained model provided [here](#) with default parameters (seeds 0 – 10000).
- **DiffProjGAN and DiffStyleGAN2** (Wang et al., 2022): We use the pre-trained model provided [here](#) and [here](#) with default parameters (seeds 0 – 10000).
- **DDPM** (Ho et al., 2020): We use the diffusers library (von Platen et al., 2022) (specifically the default DDIM pipeline) with the model provided [here](#).
- **ImprovedDDPM** (Nichol & Dhariwal, 2021): We use the model provided [here](#) with 1000 diffusion steps, a timestep respacing of 100 and DDIM (Song et al., 2020) (otherwise we use default parameters).
- **NVAE** (Vahdat & Kautz, 2020): We use the checkpoint provided [here](#) with default parameters.

ImageNet models.

- **StudioGAN** (Kang et al., 2022): We take the pre-trained models provided [here](#). Specifically, if there are multiple training runs, we take the latest one and use the weights from the best checkpoint. The models that were reproduced by StudioGAN that we used are: ReACGAN (Kang et al., 2021), BigGAN (Brock et al., 2018), SNGAN (Miyato et al., 2018), ContraGAN (Kang & Park, 2020), StyleGAN2 (Karras et al., 2020b), StyleGAN3 (Karras et al., 2021) and SAGAN (Zhang et al., 2019a).
- **StyleGANXL** (Sauer et al., 2022): We use the pre-trained model provided [here](#) and generate 10000 samples with default parameters (seeds 0 – 10000).
- **ADM** (Dhariwal & Nichol, 2021): We use the checkpoint provided [here](#) with 1000 diffusion steps, a timestep respacing of 100 and DDIM (otherwise we use default parameters).

LSUN models.

- **ProjGAN** (Sauer et al., 2021): We use the pre-trained models provided [here](#) with default parameters (seeds 0 – 10000).
- **DiffProjGAN and DiffStyleGAN2** (Wang et al., 2022): We use the checkpoints provided [here](#) and [here](#) with default parameters (seeds 0 – 10000).
- **ADM** (Dhariwal & Nichol, 2021): We use the checkpoint provided [here](#) with 1000 diffusion steps, a timestep respacing of 100 and DDIM (otherwise we use default parameters).
- **ImprovedDDPM** (Nichol & Dhariwal, 2021): We use the checkpoint provided [here](#) with 1000 diffusion steps, a timestep respacing of 100 and DDIM (otherwise we use default parameters).
- **Latent Diffusion** (Rombach et al., 2022): We use the checkpoint provided [here](#) with 200 diffusion steps, DDIM and an η of 1.

E. Proof of Proposition 1

We now prove our Proposition 1 from the main paper.

Proposition 1. *For each $\mathbf{x}_k^{\text{gen}} \in \{\mathbf{x}_i^{\text{train}}\}_{i=1}^n$ we have that $\hat{\sigma}_j^2 = 0$ where $\hat{\sigma}^2$ is a solution of Eq. 4.*

Proof. Let us consider $\mathbf{x}_k^{\text{gen}} \in \{\mathbf{x}_i^{\text{gen}}\}_{i=1}^m \cap \{\mathbf{x}_i^{\text{train}}\}_{i=1}^n$, we have that there exists l such that $\mathbf{x}_k^{\text{gen}} = \mathbf{x}_l^{\text{train}}$ thus

$$\begin{aligned} & \sum_{i=1}^n \log \sum_{j=1}^m \frac{\exp\left(\frac{-\|\varphi(\mathbf{x}_j^{\text{gen}}) - \varphi(\mathbf{x}_i^{\text{train}})\|^2}{2\sigma_j^2}\right)}{\sigma_j^d} \\ & \geq \frac{\exp\left(\frac{-\|\mathbf{x}_k^{\varphi(\text{gen})} - \varphi(\mathbf{x}_l^{\text{train}})\|^2}{2\sigma_j^2}\right)}{\sigma_k^d} \\ & = \sigma_k^{-d} \xrightarrow{\sigma_k \rightarrow 0} \infty \end{aligned}$$

□